

Kinetic magnetism and stripe order in the doped AFM bosonic $t - J$ model

Timothy J. Harris,^{1,2,*} Ulrich Schollwöck,^{1,2} Annabelle Bohrdt,^{2,3} and Fabian Grusdt^{1,2,†}

¹*Department of Physics and Arnold Sommerfeld Center for Theoretical Physics (ASC),
Ludwig-Maximilians-Universität München, Theresienstr. 37, München D-80333, Germany*

²*Munich Center for Quantum Science and Technology (MCQST), Schellingstr. 4, München D-80799, Germany*

³*Institute for Theoretical Physics, University of Regensburg, Regensburg D-93053, Germany*

(Dated: October 2, 2024)

Unraveling the microscopic mechanisms governing the physics of doped quantum magnets is a central challenge in strongly correlated many-body physics. Quantum simulation platforms, e.g. ultracold atoms trapped in optical lattices or tweezer arrays, offer an exciting pathway to investigate the interplay between spin and charge motion, thereby providing an avenue to addressing longstanding questions such as the nature of charge pairing in high-temperature superconductors. Here, in a new twist, we seek to disentangle the role of particle statistics in the physics of strongly correlated systems by exploring the strong coupling limit of doped bosonic quantum magnets, specifically the antiferromagnetic (AFM) bosonic $t - J$ model. We perform large-scale density matrix renormalization group (DMRG) calculations to map out the phase diagram of the AFM bosonic $t - J$ model on the 2D square lattice at finite doping. We find that in the low doping regime, bosonic holes tend to form partially-filled stripes, akin to those observed in high- T_c cuprates. As doping increases beyond a critical value $\delta \gtrsim \delta_{\text{FP}}^*(\delta_{\text{FM}}^*)$, a transition occurs between AFM and ferromagnetic (FM) ground states, driven by the competition between Heisenberg-type AFM and Nagaoka-type FM mediated by the motion of mobile bosonic holes. In the high doping or large t/J limit, the system evolves into a fully-polarized SU(2) ferromagnet, consistent with a phase transition linked to Nagaoka polarons. Our findings shed light on the role of particle statistics in strongly correlated quantum matter and connect to phases in the 2D Fermi-Hubbard and $t - J$ models. Our results may be realized in state-of-the-art quantum simulation experiments with bosonic quantum gas microscopes, paving the way for further exploration of doped bosonic quantum magnets.

Introduction.—Developing a precise theoretical description of the complex interplay between spin and charge degrees-of-freedom in doped Mott insulators remains a key challenge at the heart of strongly correlated many-body physics [1]. To date, the majority of the theoretical discussions have focussed on two paradigmatic Hamiltonians, namely the two-dimensional (2D) Fermi-Hubbard and $t - J$ models, which are believed to capture the essential low-energy physics of high- T_c cuprate compounds [2, 3]. However, in strongly correlated electronic systems, it currently remains unclear which portion of the observed phenomenology [4], exhibiting rich intertwined phases such as superconducting, stripe or charge-density wave (CDW) orders, can be attributed to the fermionic nature of the charge carriers, as compared to the competition between motional and magnetic degrees of freedom.

Analog quantum simulation platforms, such as ultracold atoms trapped in optical lattices or tweezer arrays, provide a flexible pathway to probe and unravel the effect of particle statistics on the competition between spin and charge motion in microscopic detail (e.g. with the aid of quantum gas microscopes [5–7]), thereby shedding new light on long-standing questions such as the nature of charge pairing in high- T_c superconductors [8, 9]. They achieve this by combining precise levels of coherent control, high fidelity state preparation and single-atom spin-resolved detection techniques [10, 11], together with the capability to extract novel multi-point correlation functions that go beyond the measurement capabilities of tra-

ditional solid-state experiments [9, 12–14]. These significant technical advances have opened new avenues toward systematically disentangling the effect of particle statistics on strongly correlated electronic phases [15], such as by studying the interplay of magnetic and motional degrees of freedom in a system of mobile bosonic holes with local AFM interactions, i.e. the AFM bosonic $t - J$ model. This direction is of particular relevance in light of recent experimental proposals to realize the AFM bosonic $t - J$ model in systems of ultracold atoms [16], polar molecules [17, 18] and Rydberg atom arrays [18].

Previous theoretical studies of the bosonic $t - J$ model have been restricted to studying lower dimensional systems, those with *partial* AFM couplings ($J_z > 0, J_\perp \leq 0$), or in the limit of high-temperature expansions [19–26]. At low densities (high doping) and weak interactions, the physics of bosonic dopants represents a radical departure from the principles of Fermi liquid theory. Indeed, as shown by Eisenberg and Lieb [27], spinful bosonic systems favor the formation of fully-polarized FM phases. However, in the strong coupling limit ($t/J \gg 1$) and for fully AFM spin-exchange interactions, the nature of the low-temperature (ground state) phase diagram at finite doping is an open question which remains largely unexplored. Our work aims to address this point by connecting known limits to the low doping behavior of the system, unveiling connections to the physics of Nagaoka ferromagnetism [28, 29] that has recently been explored in quantum simulations of the triangular lattice Hubbard

model in both ultracold fermionic systems [30, 31] and moiré heterostructures [32–34].

In this work, we extend the phase diagram of the AFM bosonic $t-J$ model on the 2D square lattice to finite doping via performing large-scale DMRG calculations [35–39] on finite-size cylinders [40]. At low doping, close to the Heisenberg AFM—which is independent of the underlying statistics of the charge carriers—our numerical simulations unveil signatures of stripe order associated with incommensurate AFM correlations, reminiscent of the physics of fermionic Hubbard and $t-J$ models [41–43]. In this regime, the ground state remains a total spin-singlet. Beyond a critical doping $\delta > \delta_{\text{PP}}^*$, we observe a transition between AFM and FM ordered ground states as a function of hole doping, signified by a departure from a spin-singlet ground state. This transition arises from the competition between Heisenberg AFM, mediated by local superexchange interactions, and Nagaoka-type FM, mediated by the kinetic motion of mobile bosonic holes. These so-called *Nagaoka polarons* appear beyond the critical doping $\delta > \delta_{\text{PP}}^*$ as regions of enhanced FM correlations in an otherwise AFM spin background, resulting in a linear suppression of strong AFM correlations as we dope away from half-filling. In the limit of large doping (dilute systems) or large t/J , the ground state becomes a fully-polarized SU(2) ferromagnet, consistent with a phase transition driven by the spatial overlap of Nagaoka polarons percolating throughout the system. Our results are summarized in Fig. 1.

The model.—We consider a model of two-component (i.e. spin-1/2) hard-core bosons on the 2D square lattice:

$$\hat{\mathcal{H}}_{t-J} = -t \sum_{\langle \mathbf{i}, \mathbf{j} \rangle} \sum_{\sigma} \hat{\mathcal{P}}_G \left(\hat{a}_{\mathbf{i}\sigma}^{\dagger} \hat{a}_{\mathbf{j}\sigma} + \text{H.c.} \right) \hat{\mathcal{P}}_G + J \sum_{\langle \mathbf{i}, \mathbf{j} \rangle} \left(\hat{\mathbf{S}}_{\mathbf{i}} \cdot \hat{\mathbf{S}}_{\mathbf{j}} + \frac{3}{4} \hat{n}_{\mathbf{i}} \hat{n}_{\mathbf{j}} \right), \quad (1)$$

where $\hat{a}_{\mathbf{i}\sigma}^{\dagger}$ ($\hat{a}_{\mathbf{i}\sigma}$) are the creation (annihilation) operators for a boson on lattice site $\mathbf{i} = (i_x, i_y)$ in spin state $\sigma = \uparrow, \downarrow$; $\hat{n}_{\mathbf{i}} = \sum_{\sigma} \hat{a}_{\mathbf{i}\sigma}^{\dagger} \hat{a}_{\mathbf{i}\sigma}$ and $\hat{\mathbf{S}}_{\mathbf{i}}$ are the local density and spin operators, respectively. Here $\langle \mathbf{i}, \mathbf{j} \rangle$ denotes nearest-neighbor (NN) lattice sites, t is the NN tunneling matrix element, J is the isotropic Heisenberg superexchange coupling and $\hat{\mathcal{P}}_G$ is the Gutzwiller projection operator which projects out all states with double occupancies. The bosonic $t-J$ model features both global SU(2) spin rotation symmetry and global U(1) particle number conservation symmetry, which we exploit in our numerical calculations [44].

In the following, we fix the total particle number $N = N_{\ell} - N_h$, where $N_{\ell} = L_x \times L_y$ is the number of lattice sites and N_h the total number of holes doped into the system (i.e. $\delta = N_h/N_{\ell}$). Moreover, we work in the regime with fully AFM spin-exchange interactions, $J > 0$, where the model exhibits a sign problem [26] and set $J = 1$.

At half-filling (i.e. $\langle \hat{n}_{\mathbf{i}} \rangle = 1, \forall \mathbf{i}$), the kinetic motion of the holes is frozen out and the ground state of the model,

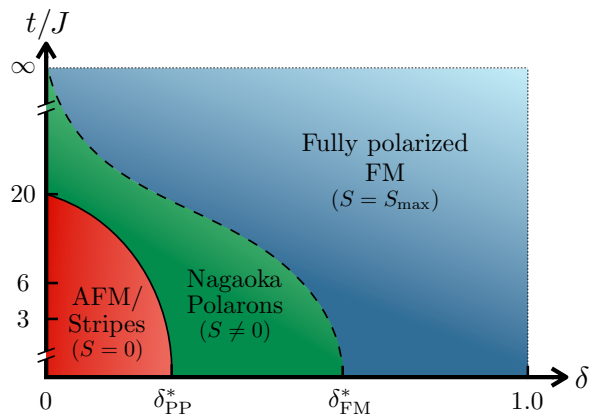


FIG. 1. Schematic phase diagram of the AFM bosonic $t-J$ model, indicating qualitatively different regimes as a function of hole doping δ and interaction strength t/J . At half-filling ($\delta = 0$), the system realizes a long-range Heisenberg AFM. As we increase hole doping, the kinetic and magnetic degrees of freedom compete, and we find a transition first to a partially polarized and then fully polarized FM phase, characterized by non-zero total spin quantum number S . Along the other axis, for $t/J \gtrsim 20$ ($t/J \rightarrow \infty$) previous numerical studies [46] have shown that a single dopant is sufficient to partially (or completely) polarize the system.

Eq. (1), is a long-range ordered Heisenberg AFM [45]. We highlight that an identical ground state is reached in the strong coupling limit of a half-filled Mott insulator for both fermionic and AFM bosonic systems. In the case of only a single dopant, it can be shown analytically that particle statistics do not play a role in determining the ground state of the system. However, for more than one hole, referred to here as the *finite doping* regime, the underlying particle statistics generally play an important part, and the physics of the system is dominated by the competition between kinetic motion of the holes and the AFM superexchange interactions.

Ground state correlations at finite doping.—We compute ground state properties of the doped bosonic $t-J$ model, Eq. (1), via applying the DMRG algorithm [35–39] on finite cylinders up to size $L_x \times L_y = 32 \times 6$ with open (closed) boundaries along the x –(y)–direction(s). We explicitly perform calculations which implement both global $U(1)_N \otimes SU(2)_S$ and $U(1)_N \otimes U(1)_{S_z}$ symmetries, in order to systematically verify the reliability of our results, and keep up to $\chi \sim 10,000$ SU(2) multiplets (equivalent to $\sim 30,000$ U(1) states) [44].

Kinetic magnetism and Nagaoka polarons.—To characterize the magnetic nature of the ground state at finite doping, we evaluate the total spin squared via summing over two-point spin-spin correlation functions:

$$\langle \hat{\mathbf{S}}^2 \rangle = \sum_{\mathbf{i}, \mathbf{j}=1}^{N_{\ell}} \langle \hat{\mathbf{S}}_{\mathbf{i}} \cdot \hat{\mathbf{S}}_{\mathbf{j}} \rangle. \quad (2)$$

Computing the correlation functions numerically allows us to access the total spin S of the ground state via the re-

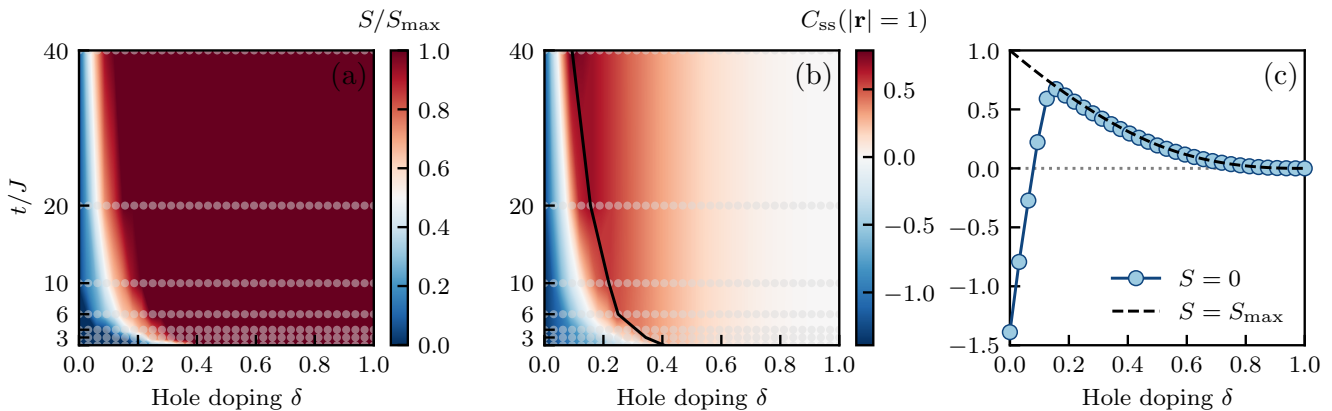


FIG. 2. (a) Heat map of the total spin quantum number S/S_{\max} as a function of hole doping δ and t/J obtained via DMRG simulations in the $S_z = 0$ symmetry sector (data points denoted by gray circles). (b) A qualitatively similar phase diagram is produced by plotting the NN spin–spin correlation function $C_{ss}(|\mathbf{r}| = 1)$, also as a function of hole doping and t/J , obtained from DRMG simulations in the $S = 0$ symmetry sector. The doping dependent peak of C_{ss} is tracked by the black line. In (c) we show a horizontal cut through the data in (b) for $t/J = 20$, illustrating a clear crossover between the AFM and FM regimes. The linear suppression of AFM correlations for $\delta \lesssim 18\%$ is consistent with the formation of Nagaoka polarons that begin to proliferate through the system. Beyond a critical doping value $\delta > \delta_{\text{FM}}^*$, the NN correlations decay as $C_{ss} \propto (1 - |\delta|)^2$, in close quantitative agreement with the correlations obtained from numerical simulations of a doped ferromagnet in the fully-polarized $S = S_{\max}$ symmetry sector (black dashed line). All DMRG calculations were performed on cylinders of size $L_x \times L_y = 16 \times 4$.

lation $\langle \hat{\mathbf{S}}^2 \rangle = S(S + 1)$. A long-range SU(2) ferromagnet is characterized by maximum total spin quantum number $S_{\max} = (N_\ell - N_h)/2$. In Fig. 2(a), we plot the evolution of total spin S/S_{\max} , normalized by its maximum value, as a function of doping for several values of t/J . We can clearly identify a regime close to half-filling ($\delta \approx 0$) where superexchange interactions dominate, resulting in a spin-singlet ground state with total spin $S = 0$.

As doping increases beyond a critical value $\delta > \delta_{\text{PP}}^*$ —which depends on the ratio t/J —the ground state transitions first to a partially-polarized (PP), and then, for $\delta > \delta_{\text{FM}}^* > \delta_{\text{PP}}^*$, to a fully-polarized (FP) ferromagnet, characterized by total spin quantum numbers $S \neq 0$ and $S = S_{\max}$, respectively. The fully-polarized phase is stable out to very large values of the doping, which is a key difference between our results compared to previous numerical studies on itinerant magnetism in geometrically frustrated fermionic systems [47].

To connect with possible experiments, we compute the connected spin–spin correlation function

$$C_{ss}(\mathbf{r}) = \frac{4}{\mathcal{N}_{\mathbf{r}}} \sum_{\mathbf{i}-\mathbf{j}=\mathbf{r}} \left(\langle \hat{\mathbf{S}}_{\mathbf{i}} \cdot \hat{\mathbf{S}}_{\mathbf{j}} \rangle - \langle \hat{\mathbf{S}}_{\mathbf{i}} \rangle \langle \hat{\mathbf{S}}_{\mathbf{j}} \rangle \right), \quad (3)$$

with normalization factor $\mathcal{N}_{\mathbf{r}}$ denoting the number of lattice sites \mathbf{i}, \mathbf{j} at a distance \mathbf{r} . In Fig. 2(b), we plot the NN correlator $C_{ss}(|\mathbf{r}| = 1)$ as a function of doping δ for several ratios of t/J . At half-filling, superexchange interactions lead to a ground state characterized by strong NN AFM correlations (i.e. $C_{ss} < 0$). However, as we increase the doping level, this negative correlation is rapidly suppressed due to the formation of Nagaoka polarons in the

system. Indeed, the NN correlations eventually turn ferromagnetic ($C_{ss} > 0$) and saturate beyond a critical doping value $\delta \approx \delta_{\text{FM}}^*$, consistent with the picture of percolating Nagaoka polarons driving a transition to a fully polarized FM phase [29]. For $\delta > \delta_{\text{FM}}^*$, the NN correlations decay as $C_{ss} \propto (1 - |\delta|)^2$, in quantitative agreement with a transition to a doped long-range SU(2) FM in this regime, as verified by corresponding DMRG calculations in the fully-polarized ($S = S_{\max}$) symmetry sector (see Fig. 2(c)). Notably, the shift of δ_{FM}^* to lower doping with increasing t/J is consistent with the Nagaoka picture of an FM ground state emerging in the limit of infinitesimal positive doping as $t/J \rightarrow \infty$ [28].

Signatures of stripe order at low doping.—In addition to signatures of kinetic magnetism and Nagaoka polarons observed in the magnetic correlations at intermediate to high doping, we also identify evidence for the emergence of partially-filled stripes in the low-doping regime where the ground state is a total spin-singlet (i.e. $0 < \delta \lesssim \delta_{\text{PP}}^*$). To investigate this, we compute the normalized hole–hole correlation function

$$C_{hh}(\mathbf{i}, \mathbf{j}) = \langle \hat{n}_{\mathbf{i}}^h \hat{n}_{\mathbf{j}}^h \rangle / \langle \hat{n}_{\mathbf{i}}^h \rangle. \quad (4)$$

The correlator C_{hh} is suppressed if the presence of a hole at lattice site \mathbf{i} makes it less likely to find a second hole at site \mathbf{j} , while C_{hh} is enhanced if it is more likely [48]. In Fig. 3, we plot C_{hh} together with the spin–spin correlations and hole density along the long (open) direction of the cylinder. In the ground state, we observe clear signatures of the formation of partially-filled stripes, indicated by (i) a periodic modulation of the hole density along the

cylinder, and (ii) the appearance of AFM domain walls at positions of maximum hole density.

The hole–hole correlations (see Fig. 3(b)) indicate that individual bosonic dopants located within a single stripe prefer to repel from one another along the periodic direction of the cylinder. While there is no spatial preference for two holes located within different stripes. This is in line with similar correlations detected in fermionic stripes on finite cylinders [49], but stands in contrast to the emergence of tightly-bound hole pairs that have been observed in previous numerical studies of paired phases in the fermionic Hubbard and $t - J$ models [49, 50].

Experimental realization.—Our study is motivated by recent experimental advances in bosonic quantum gas microscopes [16] and Rydberg tweezer arrays [18]. Here we outline a scheme to adiabatically prepare strongly correlated many-body states of doped bosonic quantum antiferromagnets in ultracold atom experiments. This approach utilizes the unique advantages of ultracold atom quantum simulators, namely the high degree of (local) control and tunability, combined with their near perfect isolation from the environment.

For simplicity, we consider a quantum gas microscope of ^{87}Rb atoms with a spin-1/2 degree of freedom encoded in a pair of hyperfine states, e.g. $|\downarrow\rangle \equiv |F=1, m_F=-1\rangle$ and $|\uparrow\rangle \equiv |F=2, m_F=2\rangle$. Ultracold bosonic atoms in optical lattices have previously been used to study spin physics [51–55]. Additionally, they possess a key advantage over fermionic species in that it is possible to generate strong locally-programmable staggered potentials which can be used to adiabatically prepare low-entropy states without crossing a phase transition.

Natively, ultracold bosons in optical lattices realize the spin-1/2 Bose-Hubbard model with (repulsive) on-site interactions $U_{\sigma\sigma'}$ between atoms and tunneling amplitude t . Working in sufficiently deep optical lattices allows to reach the strong coupling limit ($U_{\sigma\sigma'} \gg t$), where the low-energy sector (i.e. without double occupancy) is effectively described by the bosonic $t - J$ model, Eq. (1), denoted here as $\hat{\mathcal{H}}(t, J)$, with *ferromagnetic* superexchange coupling $J = -4t^2/U < 0$ [56]. However, by leveraging the bounded nature of the spectrum in the low-energy sector, it is possible to “flip” the sign of the Hamiltonian in order to experimentally realize antiferromagnetic coupling between bosons [57–59]. This amounts to observing that the highest energy eigenstate of the FM bosonic $t - J$ model $\hat{\mathcal{H}}(t, J)$, corresponds to the ground state of the AFM $t - J$ Hamiltonian $-\hat{\mathcal{H}}(t, J) = \hat{\mathcal{H}}(t, -J)$ where we have exploited the fact that on a bipartite lattice the sign of the tunneling matrix element t can be exchanged via a local gauge transformation $\hat{a}_{j\sigma} \rightarrow (-1)^j \hat{a}_{j\sigma}$ [16], leaving the overall physics invariant.

In practice, implementing this scheme requires preparation of the highest excited eigenstate of the FM Hamiltonian $\hat{\mathcal{H}}(t, J)$ with high fidelity. At half-filling, this can be achieved via locally projecting a strong staggered field

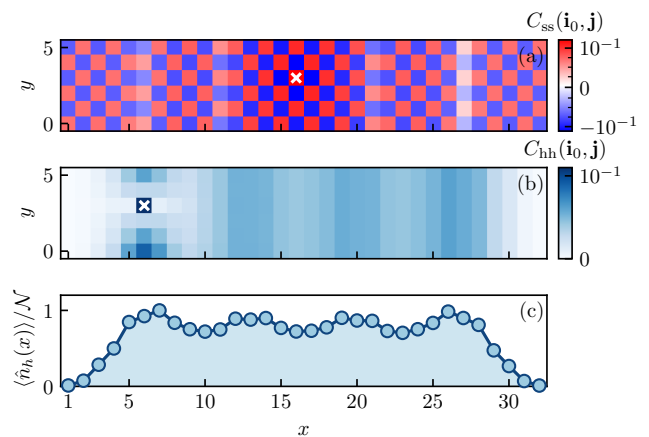


FIG. 3. (a) Connected spin–spin correlations $C_{ss}(\mathbf{i}_0, \mathbf{j})$ w.r.t. reference site $\mathbf{i}_0 = (16, 3)$ for a 32×6 cylinder with $N_h = 8$ (i.e. $\delta = 4.2\%$) and $t/J = 3$ in the $S = 0$ symmetry sector. Correlations are color coded using a symmetric logarithmic scale, with linear interpolation between -10^{-4} and 10^{-4} . Domain walls in the AFM background appear as neighboring pairs of lattice sites with like-signed correlations in the horizontal direction. (b) Normalized hole–hole correlation function $C_{hh}(\mathbf{i}_0, \mathbf{j})$ w.r.t. the reference site $\mathbf{i}_0 = (6, 3)$. Within a stripe holes repel one another around the periodic direction of the cylinder. (c) Mean hole density $\langle \hat{n}_i^h(x) \rangle = \sum_{y=1}^{L_y} \langle \hat{n}_i^h(x, y) \rangle$, normalized by maximum value, as a function of position along the long (open) direction of the cylinder. The density profile exhibits a periodic modulation, with hole rich regions corresponding to positions of AFM domain walls identified in (a). Reference sites are denoted by white crosses in (a) and (b).

of strength $h_z \gg J$ onto the lattice for which a 2D Néel state corresponds to the highest excited eigenstate of the system. Adiabatically ramping the field $h_z \rightarrow 0$ then prepares the highest excited eigenstate. To prepare ground states of doped bosonic quantum AFMs imposes further constraints on the state preparation protocol, additionally requiring that all holes in the system can be locally controlled [16]. In this way, striped ground states could also be directly prepared.

Outlook.—In this letter, we have analyzed the delicate interplay between kinetic and magnetic exchange mechanisms in the phase diagram of the doped AFM bosonic $t - J$ model. We identified a clear crossover from AFM to FM ordered ground states as a function of both doping and t/J , driven by the proliferation of Nagaoka polarons through the system. Additionally, we unveiled signatures of partially-filled stripe order in the low-doping regime, providing further evidence of a connection between our model and the strongly correlated phases of the fermionic Hubbard and $t - J$ models. Our results may be observed in state-of-the-art quantum simulation platforms, including quantum gas microscopes of ultracold neutral atoms in optical lattices, as well as Rydberg and polar molecule tweezer arrays [18].

Future work may include extending our results to finite temperatures ($T > 0$), thereby quantifying the effects of

thermal fluctuations on the observed phase diagram of the doped AFM bosonic t - J model, and exploring possible connections between low-temperature striped phases and the emergence of a pseudogap in doped bosonic systems [60–62]. From a practical perspective, it would also be interesting to investigate the effect of hole-magnon couplings in the system [55, 63], as well as the feasibility of approaches utilizing tools such as engineered dissipation [64–68] and adiabatic cooling schemes [16, 69–73] to prepare strongly correlated many-body states of doped bosonic AFMs in experiment.

Note added.—During preparation of this manuscript, we became aware of a closely related work by Zhang *et al.* [74], in which they use DMRG to explore the phase diagram of the AFM bosonic t - J model. In contrast to our study, the authors focus on cylinders of width $L_y = 4$ for which they find a pair-density wave with commensurate AFM order instead of the striped phase with incommensurate AFM order that we report in cylinders of width $L_y = 6$.

We wish to thank Tizian Blatz, Immanuel Bloch, Antoine Browaeys, Lukas Homeier, Hannah Lange, Sebastian Paeckel, Lode Pollet, Henning Schläömer, David Wei and Johannes Zeiher for valuable discussions. This research was supported by the Deutsche Forschungsgemeinschaft (DFG, German Research Foundation) under Germany’s Excellence Strategy EXC-2111 Grant No. 390814868 and the European Research Council (ERC) under the European Union’s Horizon 2020 research and innovation programme (Grant Agreement No. 948141), ERC Starting Grant SimUcQuam. T.J.H acknowledges funding by the Munich Quantum Valley (MQV) doctoral fellowship program, which is supported by the Bavarian state government with funds from the Hightech Agenda Bayern Plus. Numerical simulations were performed on the Arnold Sommerfeld Center for Theoretical Physics High-Performance Computing cluster and the KCS cluster at the Leibniz Supercomputing Center (LRZ).

* Tim.Harris@physik.uni-muenchen.de

† Fabian.Grusdt@physik.uni-muenchen.de

- [1] P. A. Lee, N. Nagaosa, and X.-G. Wen, Doping a Mott insulator: Physics of high-temperature superconductivity, *Rev. Mod. Phys.* **78**, 17 (2006).
- [2] V. J. Emery, Theory of high- T_c superconductivity in oxides, *Phys. Rev. Lett.* **58**, 2794 (1987).
- [3] F. C. Zhang and T. M. Rice, Effective Hamiltonian for the superconducting Cu oxides, *Phys. Rev. B* **37**, 3759 (1988).
- [4] B. Keimer, S. A. Kivelson, M. R. Norman, S. Uchida, and J. Zaanen, From quantum matter to high-temperature superconductivity in copper oxides, *Nature* **518**, 179 (2015).
- [5] C. Gross and I. Bloch, Quantum simulations with ultracold atoms in optical lattices, *Science* **357**, 995 (2017).
- [6] C. Gross and W. S. Bakr, Quantum gas microscopy for single atom and spin detection, *Nat. Phys.* **17**, 1316 (2021).
- [7] A. Bohrdt, L. Homeier, C. Reinmoser, E. Demler, and F. Grusdt, Exploration of doped quantum magnets with ultracold atoms, *Ann. Phys.* **435**, 168651 (2021).
- [8] A. Bohrdt, L. Homeier, I. Bloch, E. Demler, and F. Grusdt, Strong pairing in mixed-dimensional bilayer antiferromagnetic Mott insulators, *Nat. Phys.* **18**, 651 (2022).
- [9] H. Schläömer, H. Lange, T. Franz, T. Chalopin, P. Bojović, S. Wang, I. Bloch, T. A. Hilker, F. Grusdt, and A. Bohrdt, Local control and mixed dimensions: Exploring high-temperature superconductivity in optical lattices (2024), [arXiv:2406.02551](https://arxiv.org/abs/2406.02551) [cond-mat, physics:quant-ph].
- [10] C. Weitenberg, M. Endres, J. F. Sherson, M. Cheneau, P. Schauß, T. Fukuhara, I. Bloch, and S. Kuhr, Single-spin addressing in an atomic Mott insulator, *Nature* **471**, 319 (2011).
- [11] J. Koepsell, S. Hirthe, D. Bourgund, P. Sompet, J. Vijayan, G. Salomon, C. Gross, and I. Bloch, Robust Bilayer Charge Pumping for Spin- and Density-Resolved Quantum Gas Microscopy, *Phys. Rev. Lett.* **125**, 010403 (2020).
- [12] T. A. Hilker, G. Salomon, F. Grusdt, A. Omran, M. Boll, E. Demler, I. Bloch, and C. Gross, Revealing hidden antiferromagnetic correlations in doped Hubbard chains via string correlators, *Science* **357**, 484 (2017).
- [13] C. S. Chiu, G. Ji, A. Bohrdt, M. Xu, M. Knap, E. Demler, F. Grusdt, M. Greiner, and D. Greif, String patterns in the doped Hubbard model, *Science* **365**, 251 (2019).
- [14] J. Koepsell, D. Bourgund, P. Sompet, S. Hirthe, A. Bohrdt, Y. Wang, F. Grusdt, E. Demler, G. Salomon, C. Gross, and I. Bloch, Microscopic evolution of doped Mott insulators from polaronic metal to Fermi liquid, *Science* **374**, 82 (2021).
- [15] E. Khatami and M. Rigol, Effect of particle statistics in strongly correlated two-dimensional Hubbard models, *Phys. Rev. A* **86**, 023633 (2012).
- [16] A. Bohrdt*, D. Wei* et al., Microscopy of bosonic charge carriers in staggered magnetic fields, in preparation (2024).
- [17] A. V. Gorshkov, S. R. Manmana, G. Chen, J. Ye, E. Demler, M. D. Lukin, and A. M. Rey, Tunable Superfluidity and Quantum Magnetism with Ultracold Polar Molecules, *Phys. Rev. Lett.* **107**, 115301 (2011).
- [18] L. Homeier, T. J. Harris, T. Blatz, S. Geier, S. Hollerith, U. Schollwöck, F. Grusdt, and A. Bohrdt, Antiferromagnetic Bosonic t - J Models and Their Quantum Simulation in Tweezer Arrays, *Phys. Rev. Lett.* **132**, 230401 (2024).
- [19] M. Boninsegni, Phase Separation in Mixtures of Hard Core Bosons, *Phys. Rev. Lett.* **87**, 087201 (2001).
- [20] M. Boninsegni, Phase separation and stripes in a boson version of a doped quantum antiferromagnet, *Phys. Rev. B* **65**, 134403 (2002).
- [21] J. Šmakov, C. D. Batista, and G. Ortiz, Stripes, Topological Order, and Deconfinement in a Planar t - J Model, *Phys. Rev. Lett.* **93**, 067201 (2004).
- [22] M. Boninsegni and N. V. Prokof’ev, Phase diagram of an anisotropic bosonic t - J model, *Phys. Rev. B* **77**, 092502 (2008).
- [23] K. Aoki, K. Sakakibara, I. Ichinose, and T. Matsui,

- Magnetic order, Bose-Einstein condensation, and superfluidity in a bosonic CP^1 model of CP^1 spinons and doped Higgs holons, *Phys. Rev. B* **80**, 144510 (2009).
- [24] Y. Nakano, T. Ishima, N. Kobayashi, K. Sakakibara, I. Ichinose, and T. Matsui, Finite-temperature phase diagram of the three-dimensional hard-core bosonic t - J model, *Phys. Rev. B* **83**, 235116 (2011).
- [25] Y. Nakano, T. Ishima, N. Kobayashi, T. Yamamoto, I. Ichinose, and T. Matsui, Finite-temperature phase diagram of two-component bosons in a cubic optical lattice: Three-dimensional t - J model of hard-core bosons, *Phys. Rev. A* **85**, 023617 (2012).
- [26] J. Dicke, L. Rammelmüller, F. Grusdt, and L. Pollet, Phase diagram of mixed-dimensional anisotropic t - J models, *Phys. Rev. B* **107**, 075109 (2023).
- [27] E. Eisenberg and E. H. Lieb, Polarization of Interacting Bosons with Spin, *Phys. Rev. Lett.* **89**, 220403 (2002).
- [28] Y. Nagaoka, Ferromagnetism in a Narrow, Almost Half-Filled s Band, *Phys. Rev.* **147**, 392 (1966).
- [29] J. P. Dehollain, U. Mukhopadhyay, V. P. Michal, Y. Wang, B. Wunsch, C. Reichl, W. Wegscheider, M. S. Rudner, E. Demler, and L. M. K. Vandersypen, Nagaoka ferromagnetism observed in a quantum dot plaquette, *Nature* **579**, 528 (2020).
- [30] M. L. Prichard, B. M. Spar, I. Morera, E. Demler, Z. Z. Yan, and W. S. Bakr, Directly imaging spin polarons in a kinetically frustrated Hubbard system, *Nature* **629**, 323 (2024).
- [31] M. Lebrat, M. Xu, L. H. Kendrick, A. Kale, Y. Gang, P. Seetharaman, I. Morera, E. Khatami, E. Demler, and M. Greiner, Observation of Nagaoka polarons in a Fermi-Hubbard quantum simulator, *Nature* **629**, 317 (2024).
- [32] Y. Tang, L. Li, T. Li, Y. Xu, S. Liu, K. Barmak, K. Watanabe, T. Taniguchi, A. H. MacDonald, J. Shan, and K. F. Mak, Simulation of Hubbard model physics in WSe_2/WS_2 moiré superlattices, *Nature* **579**, 353 (2020).
- [33] L. Ciorciaro, T. Smoleński, I. Morera, N. Kiper, S. Hiestand, M. Kroner, Y. Zhang, K. Watanabe, T. Taniguchi, E. Demler, and A. İmamoğlu, Kinetic magnetism in triangular moiré materials, *Nature* **623**, 509 (2023).
- [34] Z. Tao, W. Zhao, B. Shen, T. Li, P. Knüppel, K. Watanabe, T. Taniguchi, J. Shan, and K. F. Mak, Observation of spin polarons in a frustrated moiré Hubbard system, *Nat. Phys.* , 1 (2024).
- [35] U. Schollwöck, The density-matrix renormalization group in the age of matrix product states, *Ann. Phys.* **326**, 96 (2011).
- [36] U. Schollwöck, The density-matrix renormalization group, *Rev. Mod. Phys.* **77**, 259 (2005).
- [37] S. R. White, Density matrix formulation for quantum renormalization groups, *Phys. Rev. Lett.* **69**, 2863 (1992).
- [38] C. Hubig, *Symmetry-protected tensor networks*, Ph.D. thesis, Ludwig-Maximilians-Universität München (2017).
- [39] C. Hubig, F. Lachenmaier, N.-O. Linden, T. Reinhard, L. Stenzel, A. Swoboda, M. Grunder, S. Mardazad, F. Pauw, and S. Paeckel, The SyTen toolkit.
- [40] E. Stoudenmire and S. R. White, Studying Two-Dimensional Systems with the Density Matrix Renormalization Group, *Annu. Rev. Condens. Matter Phys.* **3**, 111 (2012).
- [41] P. Corboz, S. R. White, G. Vidal, and M. Troyer, Stripes in the two-dimensional t - J model with infinite projected entangled-pair states, *Phys. Rev. B* **84**, 041108 (2011).
- [42] B.-X. Zheng, C.-M. Chung, P. Corboz, G. Ehlers, M.-P. Qin, R. M. Noack, H. Shi, S. R. White, S. Zhang, and G. K.-L. Chan, Stripe order in the underdoped region of the two-dimensional Hubbard model, *Science* **358**, 1155 (2017).
- [43] M. Qin, T. Schäfer, S. Andergassen, P. Corboz, and E. Gull, The Hubbard Model: A Computational Perspective, *Annu. Rev. Condens. Matter Phys.* **13**, 275 (2022).
- [44] See Supplementary Material for numerical details.
- [45] P. Fazekas, *Lecture Notes on Electron Correlation and Magnetism* (WORLD SCIENTIFIC, 1999).
- [46] S. R. White and I. Affleck, Density matrix renormalization group analysis of the Nagaoka polaron in the two-dimensional t - J model, *Phys. Rev. B* **64**, 024411 (2001).
- [47] I. Morera and E. Demler, Itinerant magnetism and magnetic polarons in the triangular lattice Hubbard model (2024), [arXiv:2402.14074 \[cond-mat\]](https://arxiv.org/abs/2402.14074).
- [48] S. Hirthe, T. Chalopin, D. Bourgund, P. Bojović, A. Bohrdt, E. Demler, F. Grusdt, I. Bloch, and T. A. Hilker, Magnetically mediated hole pairing in fermionic ladders of ultracold atoms, *Nature* **613**, 463 (2023).
- [49] T. Blatz, U. Schollwöck, F. Grusdt, and A. Bohrdt, Two-dopant origin of competing stripe and pair formation in Hubbard and t - J models (2024), [arXiv:2409.18131 \[cond-mat, physics:quant-ph\]](https://arxiv.org/abs/2409.18131).
- [50] S. R. White and D. J. Scalapino, Hole and pair structures in the t - J model, *Phys. Rev. B* **55**, 6504 (1997).
- [51] S. Trotzky, P. Cheinet, S. Fölling, M. Feld, U. Schnorrberger, A. M. Rey, A. Polkovnikov, E. A. Demler, M. D. Lukin, and I. Bloch, Time-Resolved Observation and Control of Superexchange Interactions with Ultracold Atoms in Optical Lattices, *Science* **319**, 295 (2008).
- [52] T. Fukuhara, P. Schauß, M. Endres, S. Hild, M. Cheneau, I. Bloch, and C. Gross, Microscopic observation of magnon bound states and their dynamics, *Nature* **502**, 76 (2013).
- [53] T. Fukuhara, A. Kantian, M. Endres, M. Cheneau, P. Schauß, S. Hild, D. Bellem, U. Schollwöck, T. Giamarchi, C. Gross, I. Bloch, and S. Kuhr, Quantum dynamics of a mobile spin impurity, *Nature Phys* **9**, 235 (2013).
- [54] S. Hild, T. Fukuhara, P. Schauß, J. Zeiher, M. Knap, E. Demler, I. Bloch, and C. Gross, Far-from-Equilibrium Spin Transport in Heisenberg Quantum Magnets, *Phys. Rev. Lett.* **113**, 147205 (2014).
- [55] P. N. Jepsen, J. Amato-Grill, I. Dimitrova, W. W. Ho, E. Demler, and W. Ketterle, Spin transport in a tunable Heisenberg model realized with ultracold atoms, *Nature* **588**, 403 (2020).
- [56] L.-M. Duan, E. Demler, and M. D. Lukin, Controlling Spin Exchange Interactions of Ultracold Atoms in Optical Lattices, *Phys. Rev. Lett.* **91**, 090402 (2003).
- [57] J. J. García-Ripoll, M. A. Martin-Delgado, and J. I. Cirac, Implementation of Spin Hamiltonians in Optical Lattices, *Phys. Rev. Lett.* **93**, 250405 (2004).
- [58] A. S. Sørensen, E. Altman, M. Gullans, J. V. Porto, M. D. Lukin, and E. Demler, Adiabatic preparation of many-body states in optical lattices, *Phys. Rev. A* **81**, 061603 (2010).
- [59] S. Braun, J. P. Ronzheimer, M. Schreiber, S. S. Hodgman, T. Rom, I. Bloch, and U. Schneider, Negative Absolute Temperature for Motional Degrees of Freedom, *Sci-*

- ence **339**, 52 (2013).
- [60] A. Wietek, Y.-Y. He, S. R. White, A. Georges, and E. M. Stoudenmire, Stripes, Antiferromagnetism, and the Pseudogap in the Doped Hubbard Model at Finite Temperature, *Phys. Rev. X* **11**, 031007 (2021).
- [61] H. Xu, C.-M. Chung, M. Qin, U. Schollwöck, S. R. White, and S. Zhang, Coexistence of superconductivity with partially filled stripes in the Hubbard model, *Science* **384**, eadh7691 (2024).
- [62] F. Šimkovic, R. Rossi, A. Georges, and M. Ferrero, Origin and fate of the pseudogap in the doped Hubbard model, *Science* **385**, eade9194 (2024).
- [63] Y. K. Lee, M. Block, H. Lin, V. Fedoseev, P. J. D. Crowley, N. Y. Yao, and W. Ketterle, Observation of spin squeezing with contact interactions in one- and three-dimensional easy-plane magnets (2024), arXiv:2409.17398 [cond-mat, physics:physics, physics:quant-ph].
- [64] B. Kraus, H. P. Büchler, S. Diehl, A. Kantian, A. Micheli, and P. Zoller, Preparation of entangled states by quantum Markov processes, *Phys. Rev. A* **78**, 042307 (2008).
- [65] F. Verstraete, M. M. Wolf, and J. Ignacio Cirac, Quantum computation and quantum-state engineering driven by dissipation, *Nature Phys* **5**, 633 (2009).
- [66] A. J. Daley, Quantum trajectories and open many-body quantum systems, *Advances in Physics* **63**, 77 (2014).
- [67] P. M. Harrington, E. J. Mueller, and K. W. Murch, Engineered dissipation for quantum information science, *Nat Rev Phys* **4**, 660 (2022).
- [68] X. Mi, A. A. Michailidis, S. Shabani, K. C. Miao, P. V. Klimov, J. Lloyd, E. Rosenberg, R. Acharya, I. Aleiner, T. I. Andersen, M. Ansmann, F. Arute, K. Arya, A. Asfaw, J. Atalaya, J. C. Bardin, A. Bengtsson, G. Bortoli, A. Bourassa, J. Bovaird, L. Brill, M. Broughton, B. B. Buckley, D. A. Buell, T. Burger, B. Burkett, N. Bushnell, Z. Chen, B. Chiaro, D. Chik, C. Chou, J. Cogan, R. Collins, P. Conner, W. Courtney, A. L. Crook, B. Curtin, A. G. Dau, D. M. Debroy, A. Del Toro Barba, S. Demura, A. Di Paolo, I. K. Drozdov, A. Dunsworth, C. Erickson, L. Faoro, E. Farhi, R. Fatemi, V. S. Ferreira, L. F. Burgos, E. Forati, A. G. Fowler, B. Foxen, É. Genois, W. Giang, C. Gidney, D. Gilboa, M. Giustina, R. Gosula, J. A. Gross, S. Habegger, M. C. Hamilton, M. Hansen, M. P. Harrigan, S. D. Harrington, P. Heu, M. R. Hoffmann, S. Hong, T. Huang, A. Huff, W. J. Huggins, L. B. Ioffe, S. V. Isakov, J. Iveland, E. Jeffrey, Z. Jiang, C. Jones, P. Juhas, D. Kafri, K. Kechedzhi, T. Khattar, M. Khezri, M. Kieferová, S. Kim, A. Kitaev, A. R. Klots, A. N. Korotkov, F. Kostritsa, J. M. Kreikebaum, D. Landhuis, P. Laptev, K.-M. Lau, L. Laws, J. Lee, K. W. Lee, Y. D. Lensky, B. J. Lester, A. T. Lill, W. Liu, A. Locharla, F. D. Malone, O. Martin, J. R. McClean, M. McEwen, A. Mieszala, S. Montazeri, A. Morvan, R. Movassagh, W. Mroczkiewicz, M. Neeley, C. Neill, A. Nersisyan, M. Newman, J. H. Ng, A. Nguyen, M. Nguyen, M. Y. Niu, T. E. O'Brien, A. Opremcak, A. Petukhov, R. Potter, L. P. Pryadko, C. Quintana, C. Rocque, N. C. Rubin, N. Saei, D. Sank, K. Sankaragomathi, K. J. Satzinger, H. F. Schurkus, C. Schuster, M. J. Shearn, A. Shorter, N. Shuttly, V. Shvarts, J. Skrzynny, W. C. Smith, R. Somma, G. Sterling, D. Strain, M. Szalay, A. Torres, G. Vidal, B. Villalonga, C. V. Heidweiller, T. White, B. W. K. Woo, C. Xing, Z. J. Yao, P. Yeh, J. Yoo, G. Young, A. Zalcman, Y. Zhang, N. Zhu, N. Zobrist, H. Neven, R. Babbush, D. Bacon, S. Boixo, J. Hilton, E. Lucero, A. Megrant, J. Kelly, Y. Chen, P. Roushan, V. Smelyanskiy, and D. A. Abanin, Stable quantum-correlated many-body states through engineered dissipation, *Science* **383**, 1332 (2024).
- [69] M. Lubasch, V. Murg, U. Schneider, J. I. Cirac, and M.-C. Bañuls, Adiabatic Preparation of a Heisenberg Antiferromagnet Using an Optical Superlattice, *Phys. Rev. Lett.* **107**, 165301 (2011).
- [70] J. Schachenmayer, D. M. Weld, H. Miyake, G. A. Siviloglou, W. Ketterle, and A. J. Daley, Adiabatic cooling of bosons in lattices to magnetically ordered quantum states, *Phys. Rev. A* **92**, 041602 (2015).
- [71] A. Venegas-Gomez, J. Schachenmayer, A. S. Buyskikh, W. Ketterle, M. L. Chiofalo, and A. J. Daley, Adiabatic preparation of entangled, magnetically ordered states with cold bosons in optical lattices, *Quantum Sci. Technol.* **5**, 045013 (2020).
- [72] H. Sun, B. Yang, H.-Y. Wang, Z.-Y. Zhou, G.-X. Su, H.-N. Dai, Z.-S. Yuan, and J.-W. Pan, Realization of a bosonic antiferromagnet, *Nat. Phys.* **17**, 990 (2021).
- [73] I. Dimitrova, S. Flannigan, Y. K. Lee, H. Lin, J. Amato-Grill, N. Jepsen, I. Čepaitė, A. J. Daley, and W. Ketterle, Many-body spin rotation by adiabatic passage in spin-1/2 XXZ chains of ultracold atoms, *Quantum Sci. Technol.* **8**, 035018 (2023).
- [74] H.-K. Zhang, J.-X. Zhang, J.-S. Xu, and Z.-Y. Weng, Quantum-interference-induced pairing in antiferromagnetic bosonic $\$t\$-\$J\$ model (2024), arXiv:2409.15424 [cond-mat, physics:quant-ph].$
- [75] C. Hubig, I. P. McCulloch, U. Schollwöck, and F. A. Wolf, Strictly single-site DMRG algorithm with subspace expansion, *Phys. Rev. B* **91**, 155115 (2015).
- [76] S. Singh, R. N. C. Pfeifer, and G. Vidal, Tensor network states and algorithms in the presence of a global U(1) symmetry, *Phys. Rev. B* **83**, 115125 (2011).
- [77] S. Singh and G. Vidal, Tensor network states and algorithms in the presence of a global SU(2) symmetry, *Phys. Rev. B* **86**, 195114 (2012).
- [78] A. Weichselbaum, Non-abelian symmetries in tensor networks: A quantum symmetry space approach, *Annals of Physics* **327**, 2972 (2012).

Supplementary Materials: Kinetic magnetism and stripe order in the doped AFM bosonic $t - J$ model

In this supplementary material, we describe in detail the numerical methods utilized in our work and provide further analysis of the convergence of our results.

Numerical simulations using DMRG

All ground state calculations in this work were performed using the DMRG algorithm [35] in its matrix product state (MPS) formulation as implemented via the SYTEN toolkit [38, 39] on finite cylinders up to size $L_x \times L_y = 32 \times 6$ with open (closed) boundaries along the x -(y -) direction(s) [40]. In particular, we utilize a combination of strictly single-site (DMRG3S) [75] and two-site (2DMRG) update schemes—scaling as $\mathcal{O}(\chi^3 dw)$ and $\mathcal{O}(\chi^3 d^2 w)$ respectively, where χ is the MPS bond dimension, d the dimension of the local Hilbert space and w is the matrix product operator (MPO) bond dimension—in order to ensure optimal convergence.

Implementation of non-Abelian symmetries

The performance of the DMRG algorithm may be greatly enhanced by exploiting any available symmetries of the Hamiltonian under consideration. In addition to Abelian symmetries that are available in standard open-source tensor network libraries, e.g. global U(1) particle number $N = \sum_{\mathbf{i}} \langle \hat{n}_{\mathbf{i}} \rangle$ and magnetization $S_z = \sum_{\mathbf{i}} \langle \hat{S}_{\mathbf{i}}^z \rangle$ conservation [76], the SYTEN toolkit also allows for flexible implementation of non-Abelian symmetries [77, 78], including global SU(2) spin-rotation symmetry corresponding to conservation of the total spin quantum number S .

The use of SU(2) spin-rotation symmetry effectively reduces the local MPS bond dimension χ_i required to complete a calculation of a given accuracy by a factor

$$\mathcal{R}_\chi = \frac{\chi_{i,\text{U}(1)}}{\chi_{i,\text{SU}(2)}} \approx \langle 2S_i + 1 \rangle, \quad (\text{S1})$$

compared to a calculation utilizing global U(1) magnetization conservation. We note that this relation is not strictly exact since $\langle S_i \rangle$ depends on the magnitude of the respective Schmidt values, while the ratio of bond dimensions do not.

In practice, for the Fermi/Bose-Hubbard and $t - J$ type Hamiltonians that are considered here, we find that this ratio is typically $\mathcal{R}_\chi \approx 3$ when working in the $S = 0$ symmetry sector (i.e. total spin-singlet). Since the computational cost of the DMRG algorithm scales as $\mathcal{O}(\chi^3)$, we can therefore extract a computational speed-up by roughly a factor ~ 20 for our calculations. Moreover, this performance advantage can be greatly amplified when considering a system whose true ground state lies in a symmetry sector with $S > 0$, e.g. ferromagnetic systems. In this work, we have explicitly performed calculations which implement both global $\text{U}(1)_N \otimes \text{SU}(2)_S$ and $\text{U}(1)_N \otimes \text{U}(1)_{S_z}$ symmetries, in order to systematically verify the reliability of our numerical results.

Analysis of convergence behavior

We initialize our simulations using a randomly generated state in the desired symmetry sector, i.e. (N, S_z) or (N, S) , before commencing our DMRG sweeps. We systematically increase the maximum bond dimension of our calculations until convergence is reached. For the ground state calculations in the main text, we utilized bond dimensions up to $\chi = 10,240$ (equivalent to $\chi \sim 30,000$ U(1) symmetric states) and obtain final truncation errors $\mathcal{T}(\epsilon) \sim 1 \times 10^{-7}$ and $\mathcal{T}(\epsilon) \sim 1 \times 10^{-6}$ for $L_y = 4$ and $L_y = 6$ width cylinders respectively. To further ensure optimal convergence, we monitor local one- and two-body observables, including the local hole density and spin expectation values as well as the hole-hole and spin-spin correlation functions.